Contents

General Considerations

The starting materials were purchased and used as received from Sigma-Aldrich and Acros. Dry solvents were purified in an MBRAUN SPS-800 and stored over 4 Å molecular sieves under a dry N_2 atmosphere. NMR spectroscopy data was acquired with a Bruker AVIII 300 MHz instrument or Bruker AVIII 400 MHz at 298 K unless otherwise stated. ^{1}H DOSY NMR experiments were recorded on a Bruker AVIII 400 MHz with samples at 50 nM concentration and tetramethylsilane standard. Electrospray ionisation (ESI) and electron impact ionisation (EI) were recorded using a Bruker micrOTOF II. Nanoelectrospray ionisation (NSI) and matrix-assisted laser desorption (MALDI) mass spectra were obtained by the EPSRC National Mass Spectrometry Facility (NMSF), Swansea, UK. Elemental microanalysis was carried out on an Exeter CE-440 Elemental Analyse. Single crystal X-ray diffraction data was acquired using a Bruker Apex-II with CCD detector operating at 173 K with Mo-K_α radiation (λ = 0.71073 Å) or Rigaku Supernova with Atlas CCD detector operating at 120 K with Cu-K_α radiation (λ = 1.54184 Å). Molecular weights (M_n) and molecular mass distributions (M_w / M_n) of polymers were determined by GPC at 35°C using THF as eluent with a flow rate of 1.0 mL min^{-1}. The measurements were performed on a Shimadzu instrument equipped with an LC-20AD pump, CTO-20A oven with two PLgel 5 μm MIXED-D 300 × 7.5 mm columns, RID-20A differential refractometer and SPD-20A UV-vis detector. The experimental values were obtained relative to a calibration curve using polystyrene standards, which were corrected by Mark-Houwink parameters and a factor of 0.58.[1]

NMR Spectroscopy

Monophenolate of **8**$(H)_3$

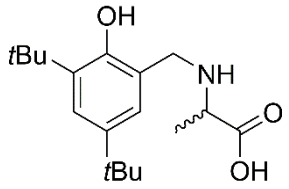

The COSY spectrum shows two sets of signals are present in the ^1H NMR of this compound in an approximate 1 : 0.25 ratio. An EXSY experiment revealed exchange between the high/low intensity signals. This is supporting evidence that there is free rotation about the methylene bridge in this compound.

^1H NMR (300 MHz, $CDCl_3$): δ 8.57 (br, 1H, PhOH), 7.19 (m, 1.5H, ArH), 6.73 (m, 1.25H, ArH), 4.92 (d, 0.25H, CH_2), 4.73 (d, 0.25H, CH_2), 4.54 (d, 1H, CH_2), 4.27 (d, 1H, CH_2), 4.20 (d, 0.25H, CH_2), 4.05 (q, 0.25H, CH), 3.81 (d, 2.5H, CH_2/CH), 3.53 (t, 1H, CH), 3.13 (d, 0.5H, CH_2), 3.01 (m, 2H, CH_2), 1.35 (s, 9H, CH_3), 1.30 (s, 9H, CH_3), 1.20 (s, 9H, CH_3); ^{13}C NMR (100.6 MHz, $CDCl_3$): δ 174.6, 153.1, 150.6, 143.0, 141.7, 137.2, 136.6, 135.9, 129.3, 129.1, 129.0, 128.6, 127.5, 126.9, 124.4, 124.0, 122.3, 121.5, 119.3, 85.0, 79.8, 77.3, 77.2, 77.0, 76.7, 65.9, 63.9, 59.4, 49.3, 36.4, 35.5, 35.0, 34.9, 34.2, 31.6, 31.5, 29.7, 29.6.

Synthetic details for ligand precursors **5**-**8**$(H)_3$

A reported procedure for the synthesis of enantiomerically pure *S*-**6**$(H)_3$ was initially followed[2] but several attempts to obtain the optically pure compound were unsuccessful. The crude mixture was purified by column chromatography in low yield and polarimetry indicated this to have racemised. This may be unsurprising as the reaction mixture is heated to reflux for several days in the presence of strong base. These harsh conditions would allow for racemisation of the amino acid through deprotonation/reprotonation of the proton adjacent to the *X* position.[3-5]

We sought to synthesise compounds **5**-**8**$(H)_3$ in higher yields using the reaction conditions previously employed in the synthesis of compounds **2**-**4**$(H)_3$.[6-9] The isolated yields for **7**$(H)_3$ and **8**$(H)_3$ were unsatisfactory (< 5 % yield). For this reason, reflux at successively higher temperatures in propan-2-ol and toluene were attempted to increase the yield but were unsuccessful in producing workable quantities of **7**$(H)_3$ or **8**$(H)_3$.

The following estimations of nuclearity are based on counting the number of signals observed in the NMR spectra and comparing this with the expected number of signals for each aggregate. These were found to correlate with the mean estimated nuclearities from ^{1}H DOSY NMR experiments, which are representative of all aggregates of different nuclearities for a complex that are present in solution. For example, the in-depth analysis of spectra for complex **11** estimates a mixture of dinuclear and trinuclear aggregates that correlates with the mean estimated nuclearity of 2.13(1) from ^{1}H DOSY NMR experiments.

Complex **10**

Due to the particular complexity of **10** in solution, the methyl groups in the R' positions were the only point of focus. Seven methyl groups coupling to the methylene and aromatic regions (COSY/ROESY) could be discerned. This revealed the possibility of trinuclear/tetranuclear aggregates existing in solution although the spread of estimated *MW*s from the DOSY NMR experiment indicates the presence of more nuclearities of aggregates (dinuclear to pentanuclear).

Complex **11**

One set of signals in methylene region are more pronounced and are similar in intensity. These doublets, corresponding to diastereotopic proton signals of the methylene bridges in the bound ligand, could be paired using COSY and ROESY NMR data. There are nine pairs (eighteen doublets) of diastereotopic signals, which would be expected for a trinuclear aggregate with nine methylene proton environments. The lower intensity peaks are under exchange with these methylene signals, which is expected due to the dynamic nature of these complexes. DOSY NMR shows a narrower distribution in comparison to the other complexes studied here. This corresponds to a trinuclear aggregate in solution as suggested by the number of methylene signals

Complex **12**

EXSY shows exchange in all regions (aromatic, methylene/isopropoxide, *tert*-butyl/isopropoxide). The number of methylene signals could be estimated by counting the number of cross coupling signals from the COSY data. A total of fifteen pairs of methylene protons was interpreted as a mixture of dinuclear and trinuclear aggregates being present in solution.

Complex *rac*-**13**

One set of pronounced signals corresponding to a mononuclear form are well-defined. However, EXSY shows exchange in all regions (aromatic, methylene/isopropoxide, *tert*-butyl/isopropoxide). The presence of more than the expected two *tert*-butyl group signals leads us to believe the exchange is between mononuclear and dinuclear forms.

Complex *rac*-**14**

This spectrum is similar in appearance to *rac*-**13**, with a set of pronounced signals corresponding to a mononuclear form are well-defined and exchange in all regions (aromatic, methylene/isopropoxide, *tert*-butyl/isopropoxide). Again, the presence of more than the expected four *tert*-butyl group signals leads us to believe the exchange is between mononuclear and dinuclear aggregates.

Figure S1. Example ^{1}H NMR spectra of complex **12**

The dynamic nature of these complexes can be suppressed by use of donor solvent or additive and monitored by NMR spectroscopy. The donor entity limits aggregation by occupying the ***L'*** site to prevent aggregation from occurring. Example spectra are provided below for complex **12**, where the number of signals in the aromatic region was successively reduced to the expected two doublets for the complex.

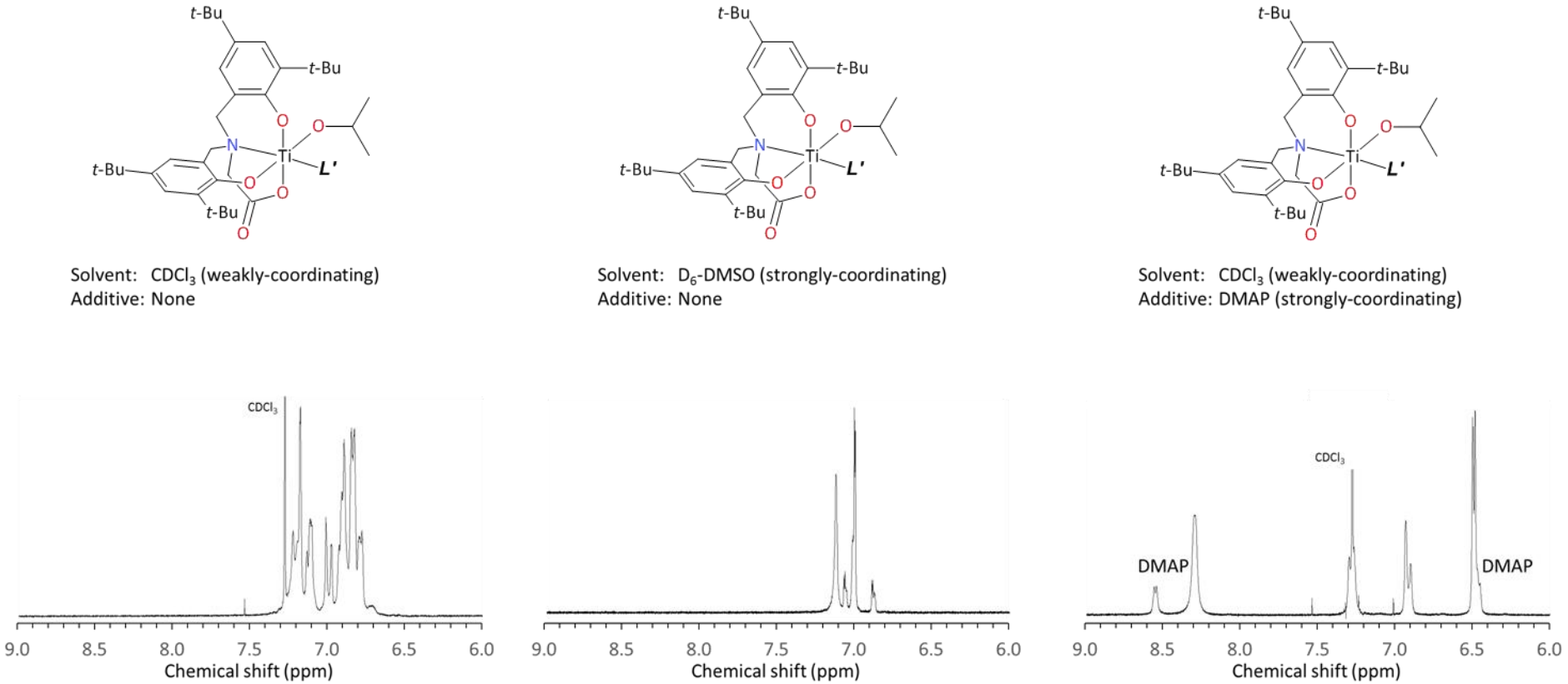

Example ^{1}H NMR spectra of the aromatic region of complex **12**. From left to right: complex chemical environments in $CDCl_3$; reduced number of chemical environments (four pairs of doublets) in D_6-DMSO; two doublets observed in $CDCl_3$ with DMAP to block the ***L'*** position.

^{1}H NMR spectra of complexes **10**-**14** with DMAP

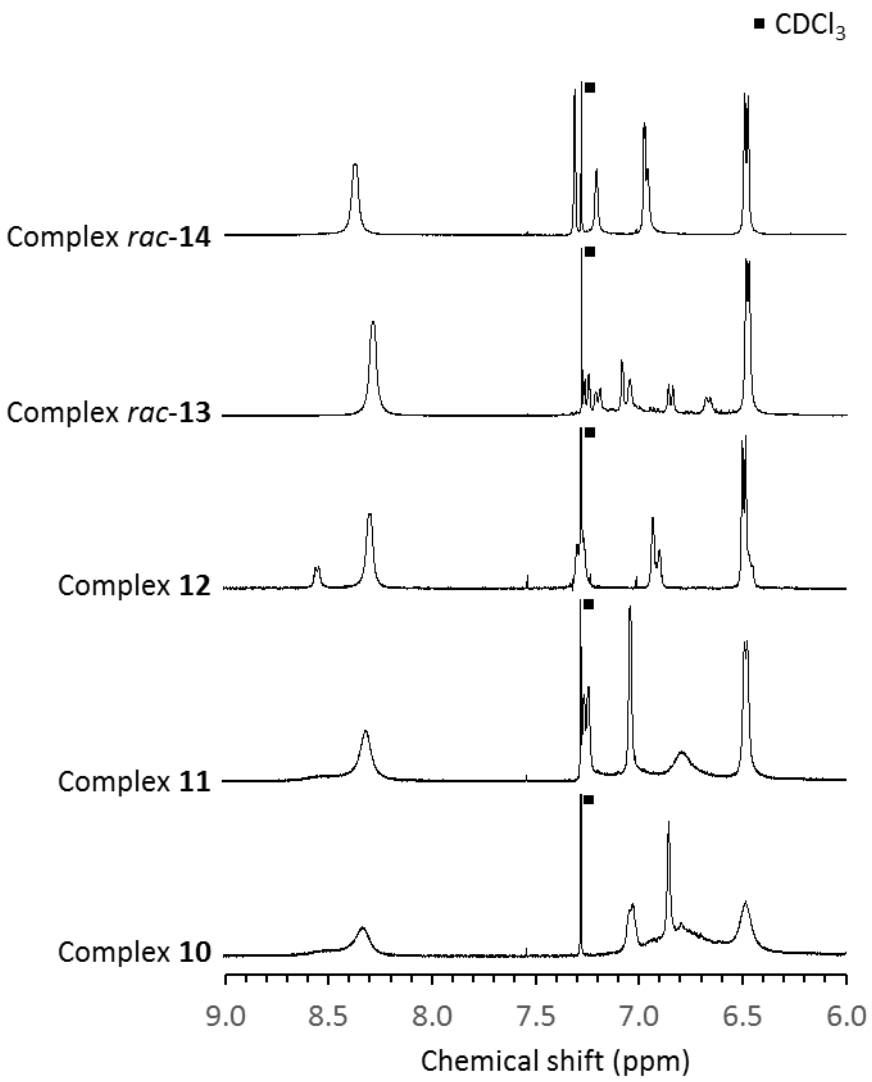

^{1}H NMR (400 MHz) spectra of complexes **10**-**14** with DMAP in $CDCl_3$ showing reduced tendency to aggregate from **10** to **14** as steric bulk increases. For complexes **10** and **11**, we observe broadened aromatic peaks at approximately 6.8 ppm that are under exchange (EXSY NMR experiment). It was also noted that the DMAP signals (approximately 6.5 ppm and 8.4 ppm) become sharper from **10** to **14**, correlating with the decreasing tendency to aggregate.

Diffusion coefficients were corrected using an internal standard (tetramethylsilane) and used to calculate estimated *MW*s according to the method published by Stalke and coworkers.[10,11] For each complex, the dataset of estimated *MW*s was counted in ranges of 50 g·mol^{-1} and converted to estimated nuclearities using the equation below:

$$\text{Estimated Nuclearity} = \frac{\text{Estimated } MW}{MW_{n=1}}$$

$$\text{where } MW_{n=1} \text{ is the molecular weight of a mononuclear unit}$$

Note: The external calibration curves (ECCs) will give accurate *MW* estimation for molecules with a molar density between 4.3 × 10^{29} g·mol^{-1}·m^{-3} and 5.9 × 10^{29} g·mol^{-1}·m^{-3}. For molecules with molar density that exceeds this range, such as complexes **10**-**14** with the presence of the titanium atom, underestimation of *MW* is expected.

This dynamic nature leads to a mean nuclearity for all aggregates in solution under equilibrium being observed, which are representative of the tendency of **10**-**14** to aggregate in solution. The dynamic nature of the aggregates in solution and the overlapping of signals in the NMR spectra can result in an average diffusion coefficient being estimated from a signal, resulting in broadening of the distributions presented here.

Individual plots of estimated nuclearity with Gaussian fit for complexes **10**-**14**

Gaussian fits of estimated nuclearities for complex **10** in solution

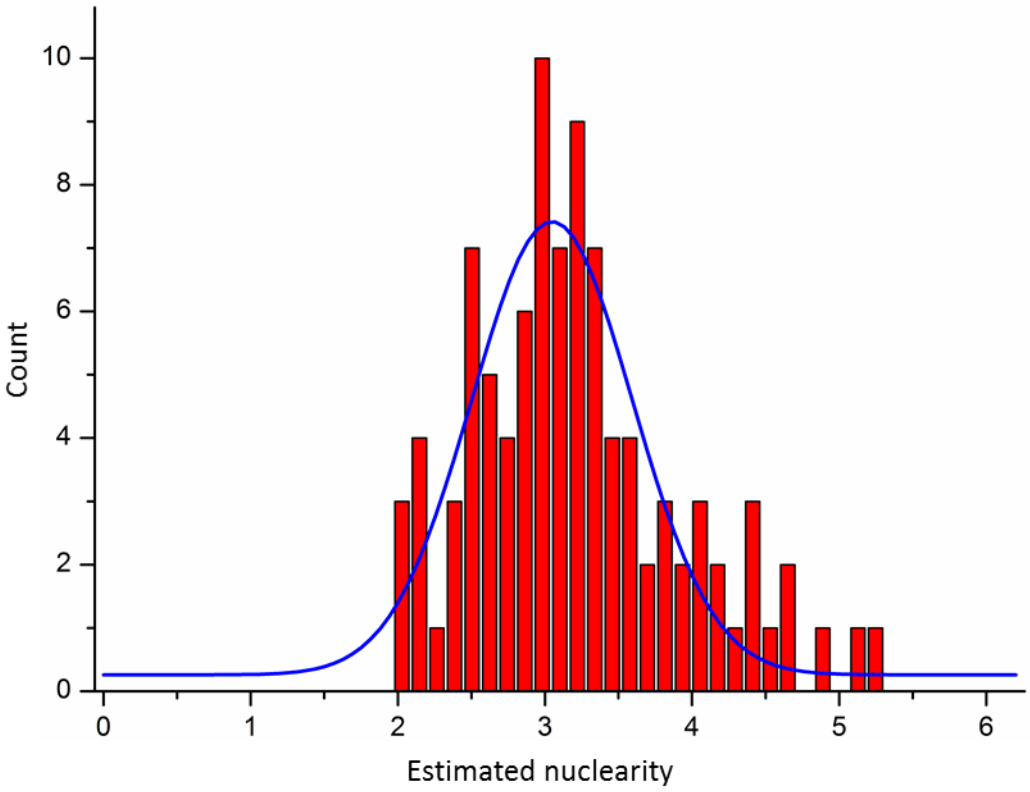

Gaussian fits of estimated nuclearities for complex **11** in solution

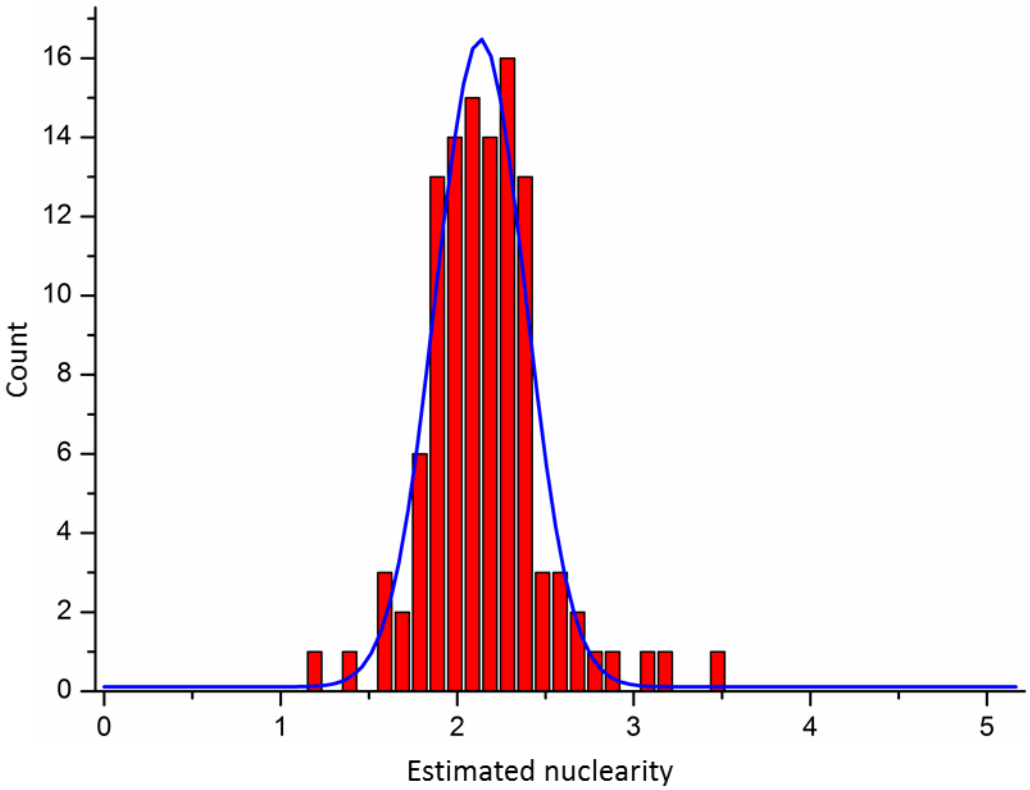

Gaussian fits of estimated nuclearities for complex **12** in solution

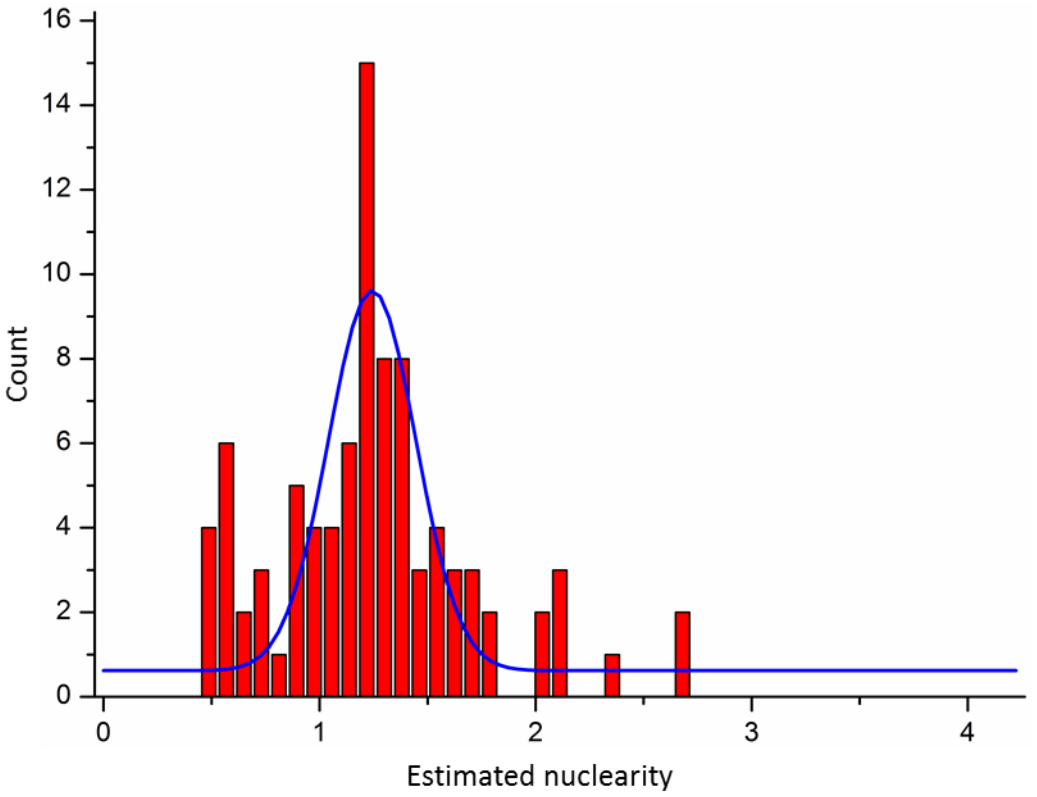

Gaussian fits of estimated nuclearities for complex *rac*-**13** in solution

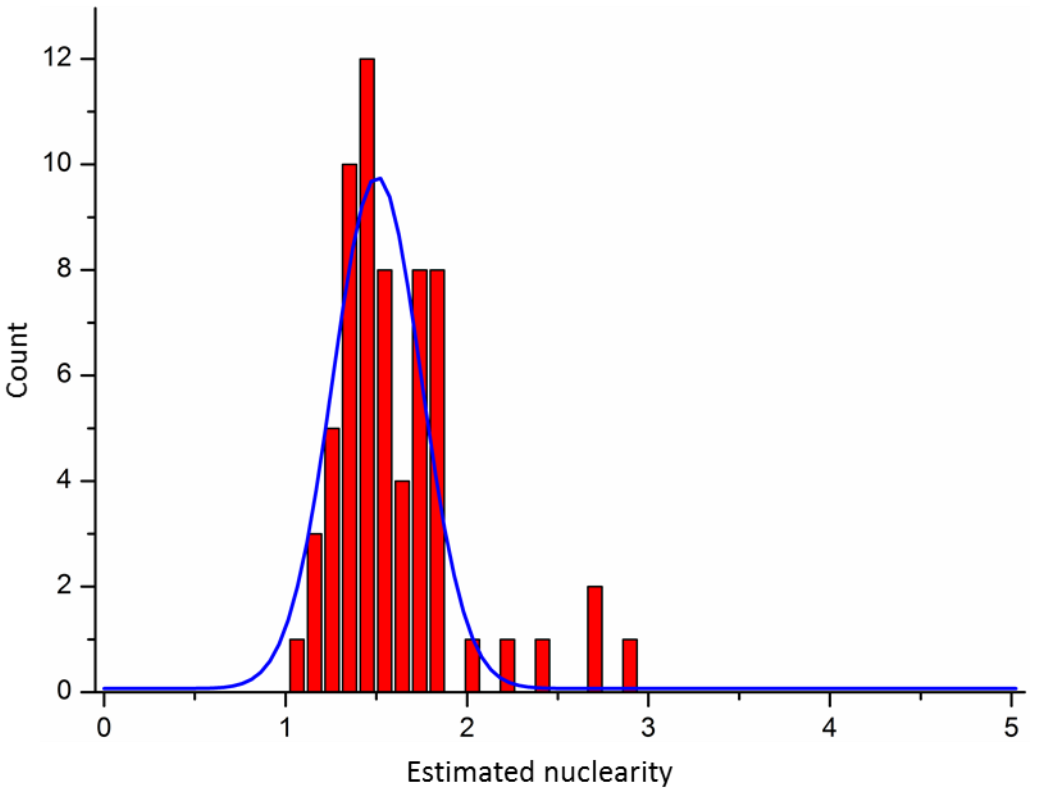

Gaussian fits of estimated nuclearities for complex *rac*-**14** in solution

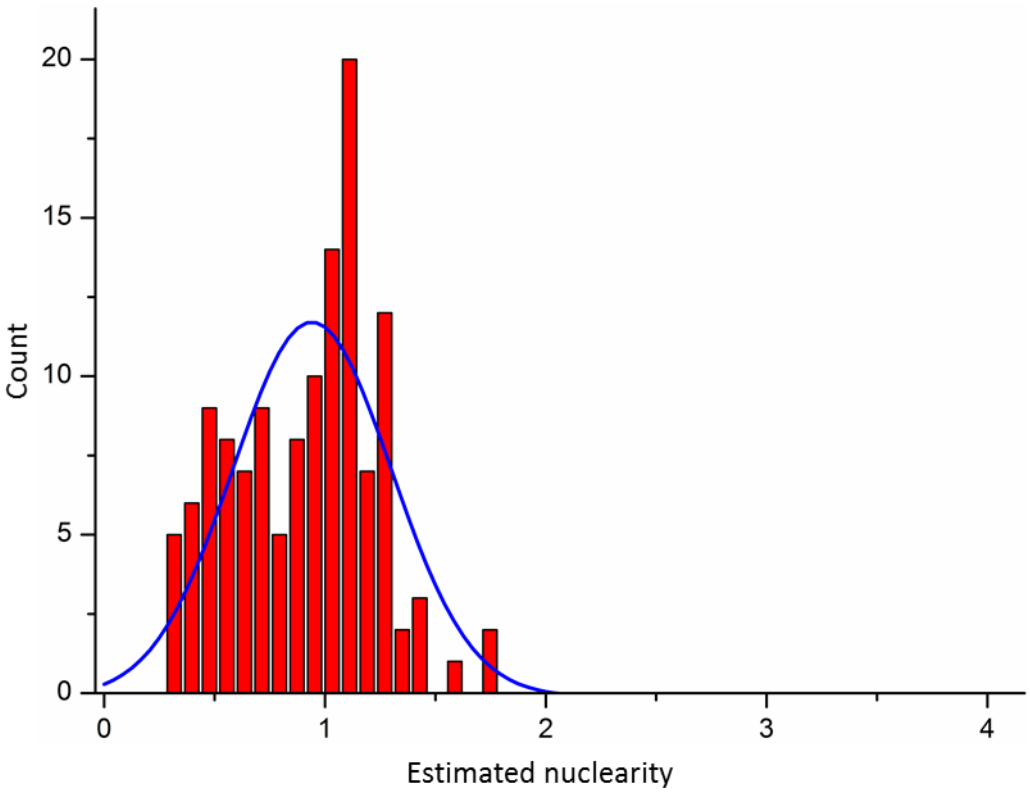

Crystal Data and Refinement Parameters

Experimental Details

Structure solution was performed using direct methods with the solving program SHELXT.[12] Structure refinement was completed with the SHELXL program[13] with the OLEX2 software package.[14] Diffuse electron density attributed to disordered solvent was refined using the SQUEEZE routine[15] for **12**$_3$(HO*i*Pr).

S-**6**(H)$_3$

Single crystals suitable for X-ray diffraction were grown by slow evaporation of a saturated solution of *rac*-**6**(H)$_3$ in methanol. The resulting large, colourless, block crystals were submitted for a SCXRD study using Cu-K_α radiation (λ = 1.54184 Å) at 120 K. The absolute configuration of the sample was obtained by anamolous dispersion.

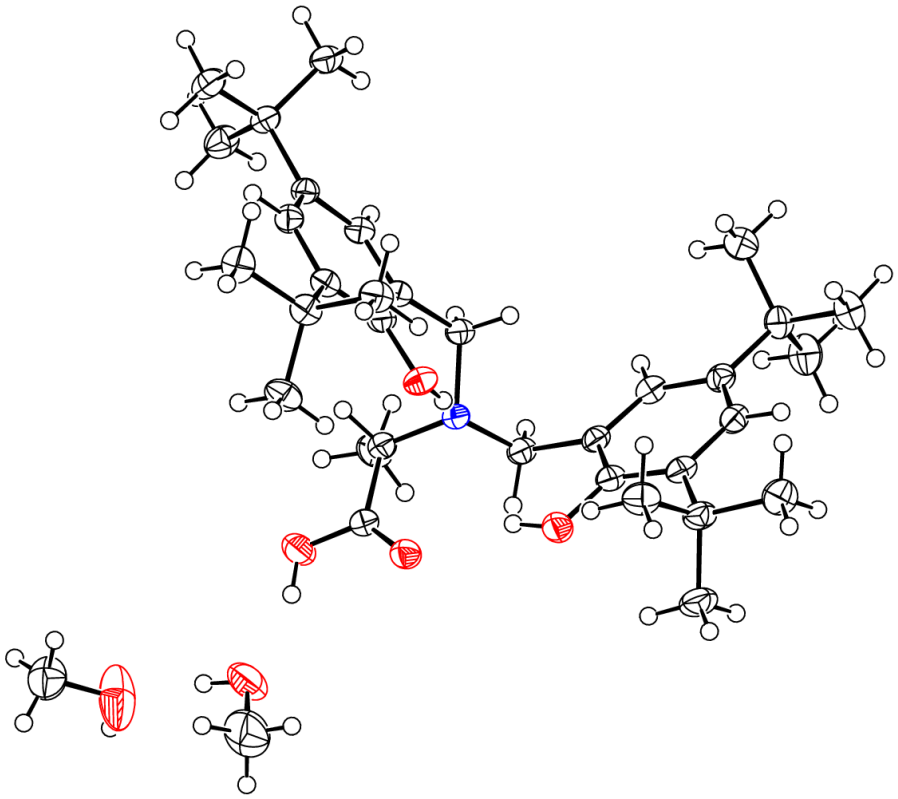

12$_3$(HO*i*Pr)

Single crystals suitable for X-ray diffraction were grown by placing a saturated solution of **12** in dry THF at –20 °C. The resulting large, orange, irregular crystals were analysed by SCXRD using Mo-K_α radiation (λ = 0.71073 Å). The crystals readily dissolved once the solution returned to room temperature. An initital dataset was obtained at 100 K with limited diffraction (*ca*. d_{min} = 1.02 Å). The experiment was repeated with further samples to give diffraction to the CCD detector limit (d_{min} = 0.78 Å). Unfortunately, these larger crystals cracked when placed under the cryostream temperatures of 100 K, 120 K and 150 K. For this reason, data collection was effected at 173 K.

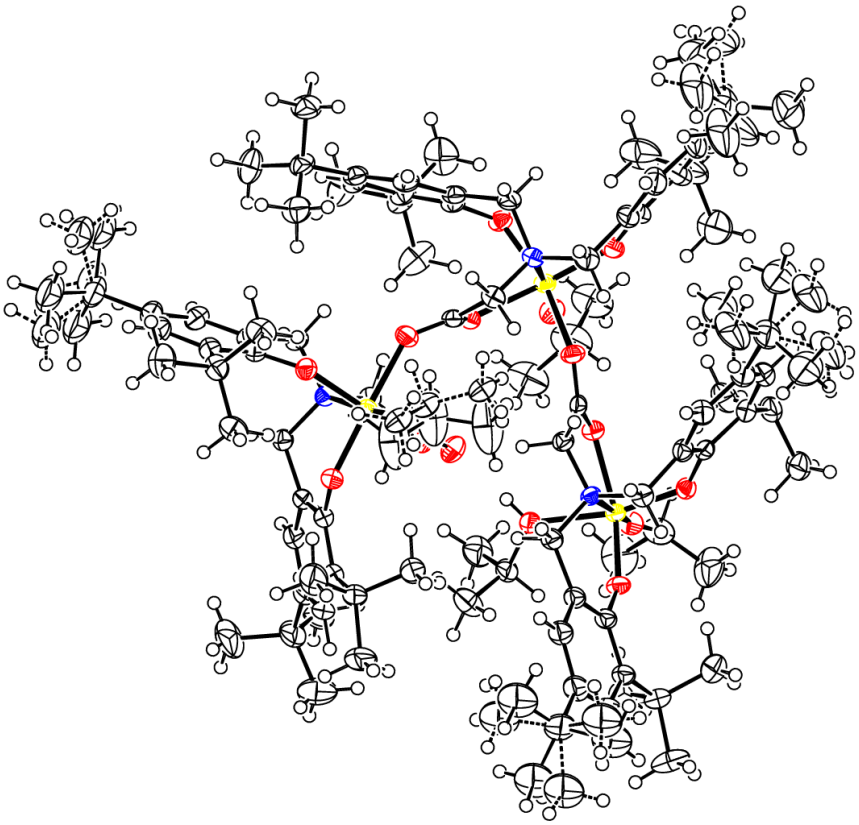

Table S1. Crystal data and structural refinement derivatives

Compound	*S*-**6**(H)$_3$	**12**$_3$(HO*i*Pr)
CCDC number	1562059	1562058
Molecular formula	$C_{35}H_{59}NO_6$	$C_{108}H_{167}N_3O_{16}Ti_3$
Molecular weight	589.83	1907.14
a (Å)	9.02228(2)	14.2420(6)
b (Å)	11.92120(2)	30.8848(14)
c (Å)	33.55580(10)	32.6649(13)
α (°)	90	90
β (°)	90	92.799(2)
γ (°)	90	90
V (Å^3)	3609.143(12)	14350.9(11)
Z	4	4
*D*c g cm^{-3}	1.086	0.883
Crystal system	Orthorhombic	Monoclinic
Space group	$P2_12_12_1$	$P2_1/n$
Temperature (K)	120.01(10)	173
Wavelength (Å)	1.54178	0.71073
Crystal size (mm)	0.303 × 0.228 × 0.139	0.45 × 0.40 × 0.40
μ(mm^{-1})	0.574	0.209
F(000)	1296	4120
ϑ limit (°)	3.94 to 76.367	0.908 to 27.226
Index ranges *hkl*	-11 ≤ *h* ≤ 10	-17 ≤ h ≤ 18
	-15 ≤ *k* ≤ 15	-39 ≤ k ≤ 39
	-42 ≤ *l* ≤ 42	-41 ≤ l ≤ 41
Reflections collected	307438	223865
Independent reflections	7534	31655
Reflections [*I*>2σ(*I*)]	7499	22417
Data/restraints/parameters	7534/0/414	31655/50/1232
Goodness-of-fit on F^2	1.057	1.040
Final *R* indices [*I*>2σ(*I*)]	R_1 = 0.0352	R_1 = 0.0695
	wR_2 = 0.0948	*w*R_2 = 0.01704
R indices (all data)	R_1 = 0.0353	R_1 = 0.01003
	wR_2 = 0.0950	*w*R_2 = 0.1872
Largest diff peak and hole (e Å^{-3})	0.25 and -0.37	1.22 and -0.80

Figure S2. Titanium-isopropanol distances

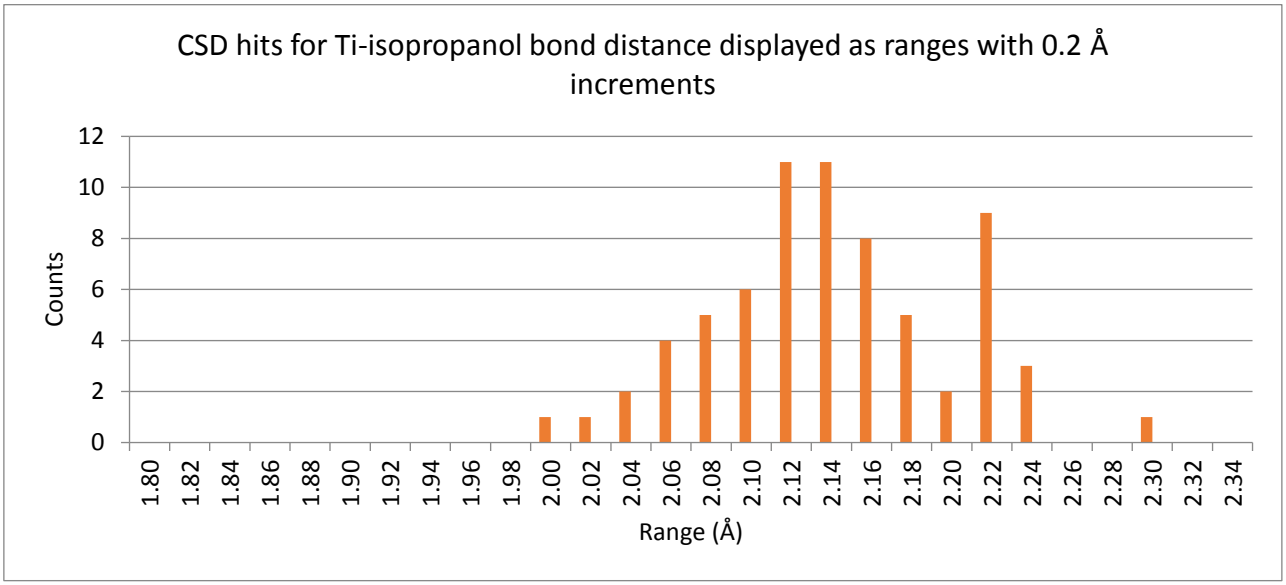

PLA Characterisation

Table S2. Comparison of data obtained for achiral versus chiral initiators the ROP of *rac*-lactide.

Initiator (achiral/chiral)	Entries (achiral/chiral)	Achiral $P_{m(CEM)}$	Chiral $P_{m(CEM)}$	Chiral $P_{m(SCM)}$
11 / *rac*-**13**	3 / 8	0.47	0.43	N/A
11 / *rac*-**13**	4 / 9	-	0.34	N/A
11 / *rac*-**13**	5 / 10	0.44	-	-
11 / *rac*-**13**	16 / 24	-	0.45	N/A
11 / *rac*-**13**	17 / 25	0.47	0.40	N/A
11 / *rac*-**13**	18 / 26	0.42	0.42	N/A
11 / *rac*-**13**	19 / 27	0.40	0.43	N/A
12 / *rac*-**14**	- / 11	-	N/A	0.61
12 / *rac*-**14**	6 / 12	0.46	N/A	0.58
12 / *rac*-**14**	20 / 28	-	-	-
12 / *rac*-**14**	21 / 29	0.41	N/A	0.68
12 / *rac*-**14**	22 / 30	0.36	N/A	0.59

Comparison of P_m data obtained for achiral versus chiral initiators **11**/*rac*-**13** and **12**/*rac*-**14** in the ROP of *rac*-lactide. P_m is the probability of isotactic enchainment, as defined in the work by Coates *et al*. where a site control mechanism (SCM)[16] and a chain end control mechanism (CEM)[17] are discussed with supporting statistics.

Figure S3. Kinetics of *rac*- or *L*-lactide consumption by *rac*-**14**

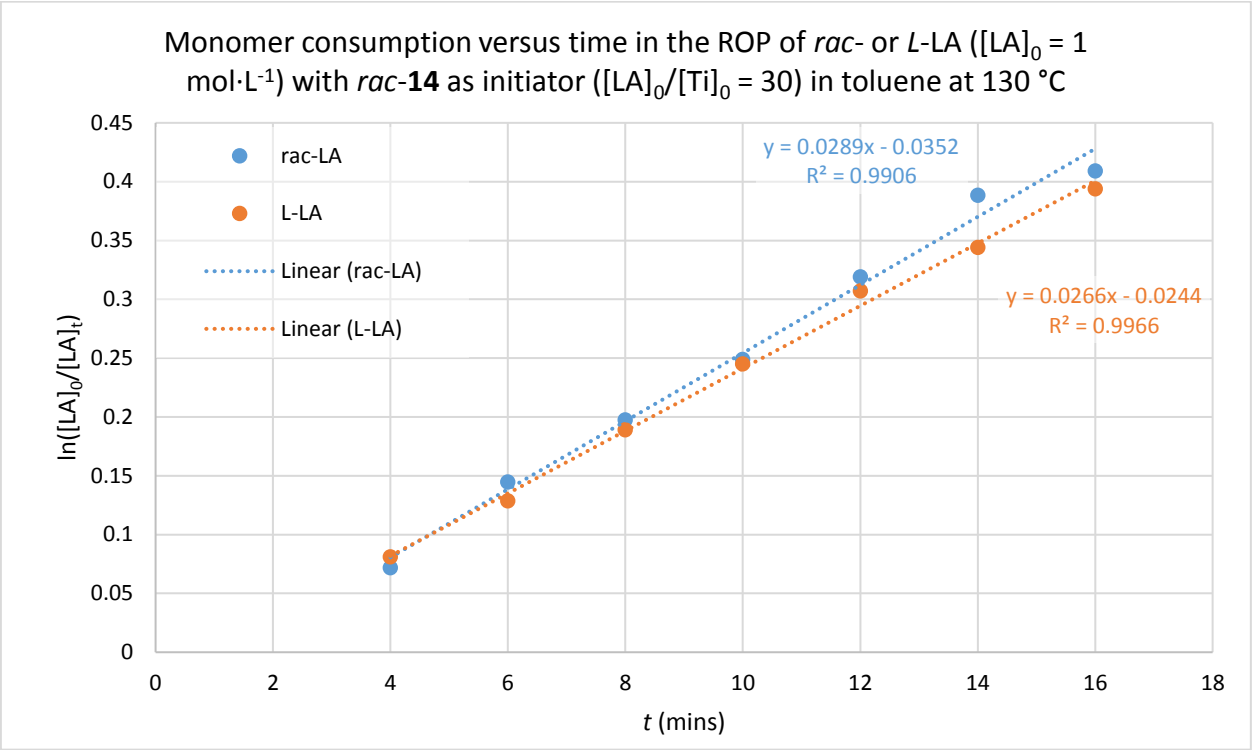

$$\ln \frac{[\mathrm{LA}]_0}{[\mathrm{LA}]_t} = k_{\mathrm{app}} t$$

where k_{app} is the applied rate constant and t is time.

Figure S4. Homonuclear Decoupled ^{1}H NMR

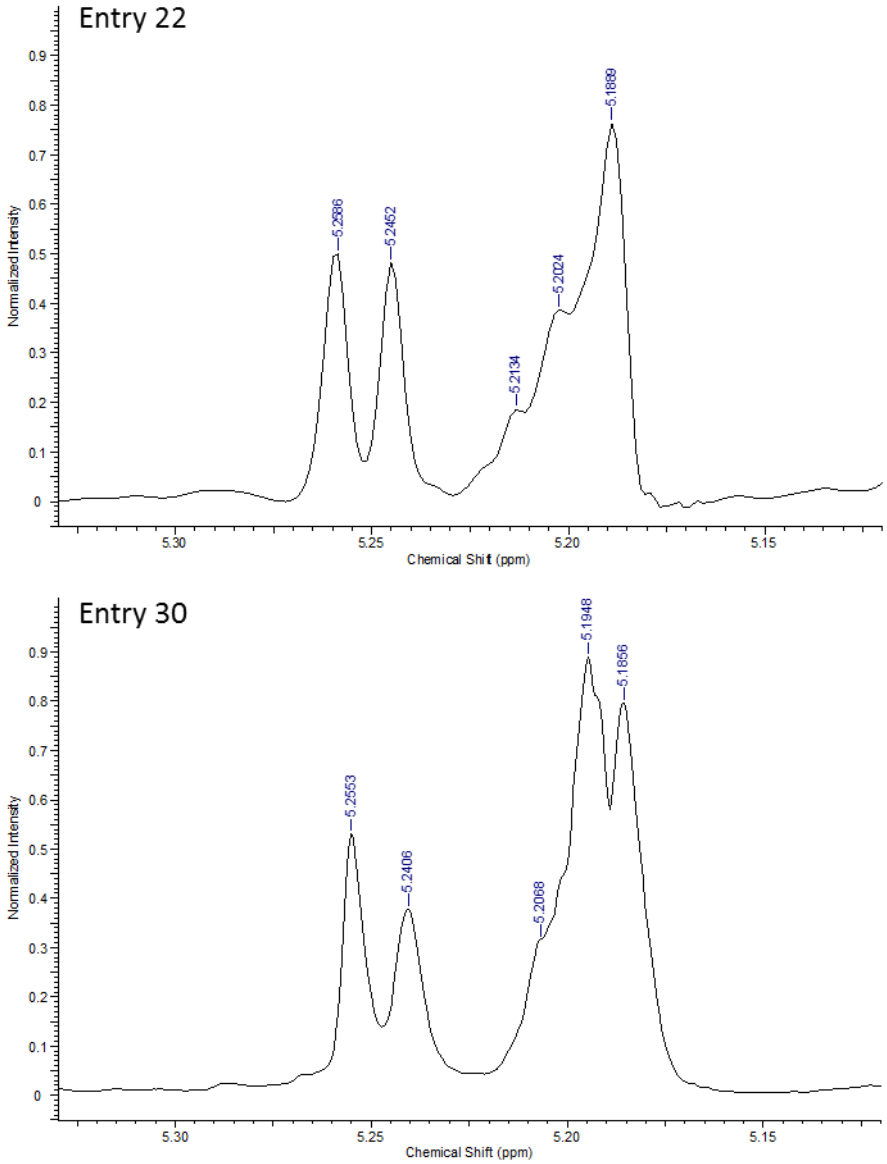

Example $\{^{1}H\}^{1}H$ spectra exemplifying the change in *mmm* tetrad intensity when using achiral (**12**, Entry 22) or chiral (*rac*-**14**, Entry 30) initiators.

Figure S5. Representative example ^{1}H NMR spectrum of polylactide (produced by initiator **11**)

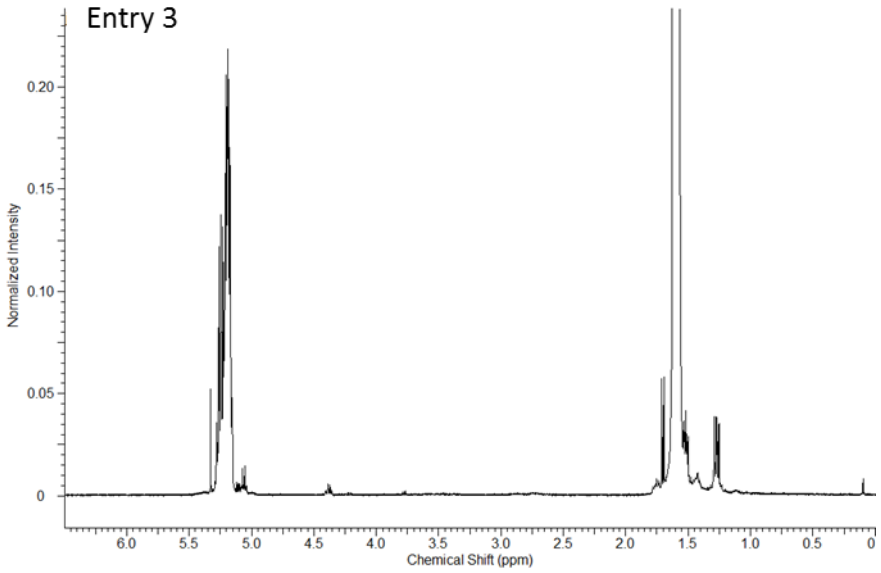

References

1. T. Biela, A. Duda and S. Penczek, *Macromol. Symp.*, 2002, **183**, 1-10.
2. S. Barroso, P. Adao, A. M. Coelho, J. C. Pessoa and A. M. Martins, *J. Mol. Catal. A: Chem.*, 2016, **412**, 107-116.
3. G. G. Smith and T. Sivakua, *J. Org. Chem.*, 1983, **48**, 627-634.
4. E. D. Stroud, D. J. Fife and G. G. Smith, *J. Org. Chem.*, 1983, **48**, 5368-5369.
5. R. Baum and G. G. Smith, *J. Am. Chem. Soc.*, 1986, **108**, 7325-7327.
6. A. S. Ceccato, A. Neves, M. A. De Brito, S. M. Drechsel, A. S. Mangrich, R. Werner, W. Haase and A. J. Bortoluzzi, *J. Chem. Soc., Dalton Trans.*, 2000, 1573-1577.
7. Y.-L. Wong, Y. Yan, E. S. H. Chan, Q. Yang, T. C. W. Mak and D. K. P. Ng, *J. Chem. Soc., Dalton Trans.*, 1998, 3057-3064.
8. Z. Taheri, B. Ghanbari and H. Hajibabaei, *Chem. Pap.*, 2014, **68**, 989-994.
9. J. M. E. P. Cols, C. E. Taylor, K. J. Gagnon, S. J. Teat and R. D. McIntosh, *Dalton Trans.*, 2016, **45**, 17729-17738.
10. R. Neufeld and D. Stalke, *Chem. Sci.*, 2015, **6**, 3354-3364.
11. S. Bachmann, R. Neufeld, M. Dzemski and D. Stalke, *Chem. Eur. J.*, 2016, **22**, 8462-8465.
12. G. M. Sheldrick, *Acta Crystallogr., Sect A: Found. Crystallogr.*, 2015, **71**, 3-8.
13. G. M. Sheldrick, *Acta Crystallogr., Sect C: Cryst. Struct. Commun.*, 2015, **71**, 3-8.
14. O. V. Dolomanov, L. J. Bourhis, R. J. Gildea, J. A. K. Howard and H. Puschmann, *J. Appl. Crystallogr.*, 2009, **42**, 339-341.
15. A. L. Spek, *Acta Crystallogr., Sect C: Cryst. Struct. Commun.*, 2015, **71**, 9-18.
16. T. M. Ovitt and G. W. Coates, *J. Am. Chem. Soc.*, 2002, **124**, 1316-1326.
17. B. M. Chamberlain, M. Cheng, D. R. Moore, T. M. Ovitt, E. B. Lobkovsky and G. W. Coates, *J. Am. Chem. Soc.*, 2001, **123**, 3229-3238.